Available online at www.springerlink.com

Acta Metall. Sin. (Engl. Lett.) Vol.26 No.3 pp. 277—284 June 2013

ACTA
METALLURGICA SINICA
(ENGLISH LETTERS)

Optimizing Mechanical Properties of $AlCoCrFeNiTi_x$ High-Entropy Alloys by Tailoring Microstructures

Yinfeng WANG[1)], *Shengguo MA*[2)], *Xiaohua CHEN*[2)], *Juyan SHI*[1)†], *Yong ZHANG*[2)] and *Junwei QIAO*[1,3)]

1) College of Materials Science and Engineering, Taiyuan University of Technology, Taiyuan 030024, China
2) State Key Laboratory for Advanced Metals and Materials, University of Science and Technology Beijing, Beijing 100083, China
3) Key Laboratory of Interface Science and Engineering in Advanced Materials, Ministry of Education, Taiyuan University of Technology, Taiyuan 030024, China

[Manuscript received 15 October 2012, in revised form 28 December 2012]

The effects of Ti addtions and the heat treatment on the mechanical properties of $AlCoCrFeNiTi_x$ (x = 0, 0.2, 0.3, 0.4 and 0.5) high-entropy alloys (HEAs) were studied. The results show that the dendrite phase with a body-centered-cubic (bcc) structure transforms into the interdendrite phase with a new bcc structure. With the increase of the Ti contents and heat-treatment temperature, the average hardness and yield strengths are greatly improved, and the highest hardness and yielding strength are 583 HV and 2.07 GPa, respectively in the investigated HEA system. The as-cast and annealed HEAs exhibit excellent mechanical properties, combining with high yielding strength and plasticity. The solid solution strengthening mechanism of Ti additions is responsible for the strengthening effect of $AlCoCrFeNiTi_x$ HEAs.

KEY WORDS: High-entropy alloy; Microstructure; Compressive property; Hardness; Heat treatment

1. Introduction

Conventional alloy system strategies have been based on one principal elements as the matrix, as in Al-, Cu-, Mg-, Ni-, Fe-(steel), and Ti-based alloys, which limits the number of alloys that can be studied and applied, even though a great amount of other elements are incorporated for the enhancement of performance. Furthermore, in order to avoid this limitation, a novel alloy approach named as high-entropy alloys (HEAs) was proposed in 2004 to broaden the alloy design[1]. By this design, HEAs were defined to contain at least five principal elements, and each has a concentration from 5 at.% to 35 at.%. It is demonstrated that HEAs usually form simple solid-solutions instead of intermetallics or complex phases under appropriate composition design[1−4]. These alloys exhibit attractive properties, such as high hardness, good thermal stability, high elevated-temperature strength and good corrosion resistance, rendering them potential applications in different aspects[5−7]. For example, Zhu *et al.*[8] found that $AlCoCrFeNiSi_x$ HEAs exhibit a high yielding strength of 1481 MPa at room temperature, which is attributed to solid solution of Si element and precipitation strengthening of a nanoscaled cellular structure. Previously, the microstructures of the as-cast AlCoCrFeNi and $AlCoCrFeNiTi_{0.5}$ have been extensively investigated, and it has been identified that a single-phase solid solution with a body-centered-cubic (bcc) structure forms for the AlCoCrFeNi HEA[9]. As a contrast, for the $AlCoCrFeNiTi_{0.5}$ HEA, the microstructure is consisted of two kinds of bcc solid solutions[1,6,10]. The evolution of microstructures of $AlCoCrFeNiTi_x$ alloy system is not clear, and the mechanical behaviors of $AlCoCrFeNiTi_x$ alloy system annealed at high temperatures are yet to be studied in detail. It is very important to optimize the mechanical properties of $AlCoCrFeNiTi_x$ alloy system for actual applications of the HEAs.

† Corresponding author. Prof., Ph.D.; Tel.: +86 351 6018051; E-mail address: shijuyan@tyut.edu.cn (Juyan SHI)

DOI: 10.1007/s40195-012-0174-5

In this study, to understand the effect of Ti additions on the mechanical properties of the $AlCoCrFeNiTi_x$ (x = 0, 0.2, 0.4, and 0.5) alloy system in the as-cast and annealed condition, the phase evolution, microstructures and mechanical properties of these alloys are discussed, which provide essentials of this HEA system for further research and applications.

2. Experimental

Alloy ingots with nominal compositions of $AlCoCrFeNiTi_x$ (x: molar ratio; x = 0, 0.2, 0.4 and 0.5, for simplicity, they are denoted as Ti0, Ti0.2, Ti0.4 and Ti0.5, respectively) were prepared by arc melting mixtures of pure metals in a Ti-gettered high-purity argon atmosphere to prevent oxidation after purging with argon three times. The ingots were then remelted at least 5 times to improve chemical homogeneity and injection cast into a water-cooled copper mould to obtain cylindrical rods with a diameter of 3 mm and a length of 70 mm alloys. The as-cast alloys were subsequently annealed at temperatures of 500, 700 and 900 °C for 2 h.

The microstructures of the as-cast and heat-treated samples were characterized by X-ray diffraction (XRD) using a PHILIPS APD-10 Diffractometer with CuK_α radiation and a scanning step of 0.05°/s from 2θ=20° to 2θ=90°. The morphologies and chemical compositions of alloys were examined with a scanning electron microscope (SEM) equipped with an energy dispersive spectrometry. Compressive tests were performed on samples of Φ3 mm× 6 mm using a material test system of servohydraulic mechanical testing machine at room temperature with a strain rate of 5×10^{-4} s^{-1}, and the morphologies of the fracture surfaces were examined by SEM. The Vickers hardness values of the alloys were measured with a Vickers hardness tester under a load 980.7 mN, and a holding time of 10 s.

3. Results and Discussion

3.1 Phase evolution

In previous studies, the microstructure of as-cast Ti0 HEA is demonstrated to be composed of a single-phase solid solution with a bcc structure, and the microstructure of as-cast Ti0.5 HEA is consisted of two kinds of bcc solid solution. The phase evolution in current alloy system was investigated.

Fig. 1 presents the XRD patterns of the as-cast and annealed $AlCoCrFeNiTi_x$ (x=0.2 and 0.4) alloys. Interestingly, all the alloys are mainly consisted of a bcc solid solution. Fig. 1(a) reveals that as-cast Ti0.2 alloy exhibits reflections of only a single bcc phase (bcc1). While for the as-cast Ti0.4 alloys in Fig. 1(b), there are reflections of another bcc phase (bcc2) besides bcc1 phase reflections. From Fig. 1(a),

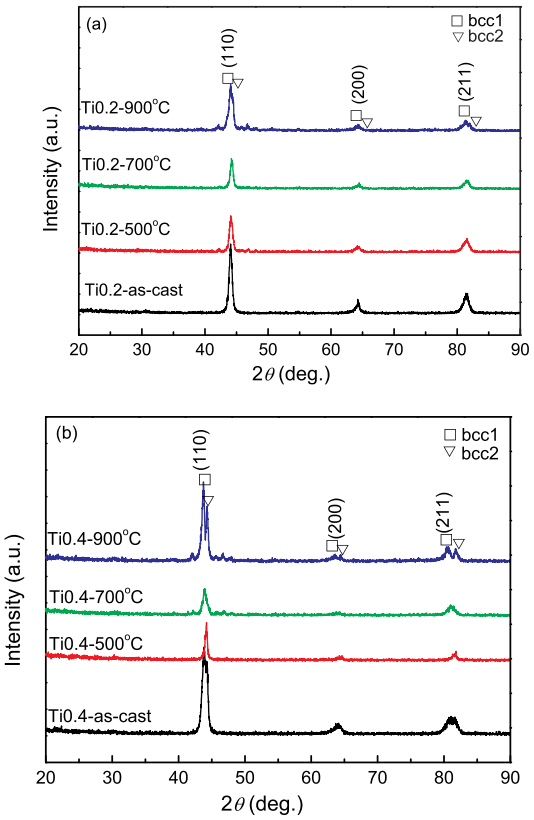

Fig. 1 XRD patterns of as-cast and annealed $AlCoCrFeNiTi_x$ alloys with different Ti additions: (a) Ti0.2; (b) Ti0.4 (bcc1 and bcc2 denoting two different phases with the same bcc structure)

and as compared with the as-cast Ti0.2 alloy, it is seen that a bcc2 phase precipitates from the bcc1 solution matrix in the annealed Ti0.2 alloys. From Fig. 1(b), it can be observed that both the as-cast and the annealed alloys are composed of two kinds of bcc solid solutions in Ti0.4 alloys, which differ only in the intensity of diffraction peaks. It can be seen that there are some peaks are overlapped originally but became separated with the temperature for both Ti0.2 and Ti0.4 alloys, which is attributed to the change of the volume fraction of two bcc phases, and the volume fraction of bcc2 increases gradually with the increase of the heat-treatment temperature. Analogous phenomena have been found in a $Cu_{0.5}CoCrFeNi$ HEA[11].

According to Boltzmann′s hypotheses, the entropy of mixing ($\Delta S_{\rm mix}$) of an N-element regular liquid can be expressed as

$$\Delta S_{\rm mix} = -R\sum_{i=1}^{n} C_i \ln C_i \qquad (1)$$

here C_i is the atomic percentage of the ith component, R is the gas constant. The entropy of mixing would reach the maximum value when the alloy is of equi-atomic ratio. Thus, the HEAs have much higher $\Delta S_{\rm mix}$ than common alloys like Mg-based alloys and intermetallics of Ti-Al, *etc.* and the $\Delta S_{\rm mix}$ can be

simplified as

$$\Delta S_{\mathrm{mix}} = R\ln(n) \tag{2}$$

In this study, bcc solid solutions rather than intermetallics formed in the present alloys. From Eq. (1), the formation superiority of solid solutions over ordered phases is attributed to the effect of the high entropy, and the entropy of mixing of Ti0, Ti0.2, Ti0.4 and Ti0.5 alloys are simply calculated to be 13.38, 14.22, 14.59 and 14.72 J/(K·mol), respectively. The high entropy of current alloys significantly lowers their Gibbs free energy, thus lowering the ordering tendency, and consequently making randomly solid solutions more easily form and more stable than ordered phases during solidification[12].

3.2 Microstructures

Fig. 2 displays the SEM images of the Ti0.2 and Ti0.4 alloys. It is found that the as-cast Ti0.2 alloy, as shown in Fig. 2(a), includes only single bcc1 phase. From Fig. 2(b), it is obvious that the average primary dendrite arm width of the alloy is about 8–12 μm, and the primary phase exhibits a typical dendritic morphology. Dendrites (gray contrast labeled as "A") and interdendrites with eutectic morphology (white contrast and black contrast, labeled as "B" in the illustration) can be observed. Besides, there are modulated structures (labeled as "C" in the inset) like the spinodal decomposition structure, as reported for Al_xCoCrCuFeNi alloys growing around the dendrite phases[13], and the characteristic width and spacing in the modulated structures are in the order of submicron meter. From Fig. 2(c), it is found that the volume fraction of the secondary phase bcc2 in Ti0.2 alloy after 700 °C heat treatment increases, compared with that of the Ti0.2 alloy annealed at 500 °C. From Fig. 2(d), it is obvious that the columnar eutectic morphology and the modulated structure in interdendrite regions grew up gradually for the Ti0.2 alloy subjected to 900 °C heat treatmentand the interdendrite precipitation ripen in the surrounded matrix. Therefore, there are plenty of dendrite phases transformed into interdendrite phases.

From the above analysis of the microstructures of Ti0.2 high-entropy alloys, it can be seen that the as-cast Ti0.2 alloy forms a single bcc1 phase, in comparison, the as-annealed Ti0.2 alloys forms a secondary phase bcc2 besides bcc1 phase, which are consistent with the XRD results.

Fig. 2(e) shows that the as-cast Ti0.4 alloy is composed of two kinds of bcc solid solutions, which are in agreement with the XRD results, and the microstructure is similar to that of annealed Ti0.2 alloys. The volume fraction of the bcc2 phase and nanoscaled modulated structure increases for the Ti0.4 alloy after 500 °C heat treatment. Fig. 2(f) exhibits the magnified SEM image of the Ti0.4 alloy annealed at 500 °C heat treatment, which indicates that the Ti0.4 alloy subjected to 500 °C heat treatment has similar microstructures to the as-cast Ti0.4 alloy. The SEM image of Ti0.4 alloy after 700 °C heat treatment is displayed in Fig. 2(g), and it is found that the volume fraction of the bcc2 phase increases continuously with the increase of the heat-treatment temperature. Fig. 2(h) presents the SEM image of the Ti0.4 alloy annealed at 900 °C heat treatment, which indicates that the size of interdendrites increase from 2 to 5 μm when annealed at 900 °C.

The chemical compositions of dendrites in Ti0.2 and Ti0.4 alloys are obtained by EDS and given in Fig. 3(a) and Fig. 3(b), respectively. Since the as-cast Ti0.2 alloy possess only single bcc1 phase and no significant compositional segregation, the compositions of dendrites of as-cast Ti0.2 alloy are not given in Fig. 3. Fig. 3(a) exhibits the composition distribution in dendrite regions of the annealed Ti0.2 alloys, and it can be obtained that Cr, Fe and Ti spread outside the dendrites with increasing temperature, leading to the increase of Al and Ni contents in the dendrite regions with the temperatures. The EDS results indicate that the dendrite regions have higher Al and Ni contents than those of the interdendrite regions, and the interdendrites have higher Cr and Fe content. It is obvious that the dendrites are bcc1 phase, and the white contrast phase in the interdendrite region with an eutectic microstructure is bcc2 phase.

Fig. 3(b) is the composition distribution in dendrite regions of the as-cast and annealed Ti0.4 alloys, which shows that Cr and Fe spread outside the dendrites with increasing temperature, resulting in the increase of Al and Ni contents in the dendrite regions. The distributing characteristics of the composition in dendrites of Ti0.4 alloys are analogous to that of the Ti0.2 alloys.

The reason of the segregation of Cr and Fe is that Cr and Fe are more electronegative than other components, thus less stable in the dendrites and were rejected into the interdendritic regions during heat treatment. Such segregation of Al and Ni could be explained by the high negative mixing enthalpy between the Al and Ni in the alloy system, *e.g.*, the negative mixing enthalpy Al-Ni rich phase is -22 kJ/mol[14] and the negative mixing enthalpy of Al with Co, Cr and Fe are -19, -10 and -11 kJ/mol[14], respectively. Therefore, the negative mixing enthalpy of these particular atoms means that Al and Ni tend to segregate in the dendrite regions and do not tend to mix with Co, Cr and Fe[15,16].

3.3 Hardness analysis

Fig. 4(a) shows the dependence of the average Vickers hardness for the AlCoCrFeNiTi_x alloys on the temperature. It can be seen that the hardness curve of the all the alloys is a parabolic type, and the maximum hardness is achieved after 700 °C heat treatment for the alloys with Ti additions, and almost all the alloys with the addition of Ti atoms have higher hardness than Ti0 alloy. This suggests that the tita-

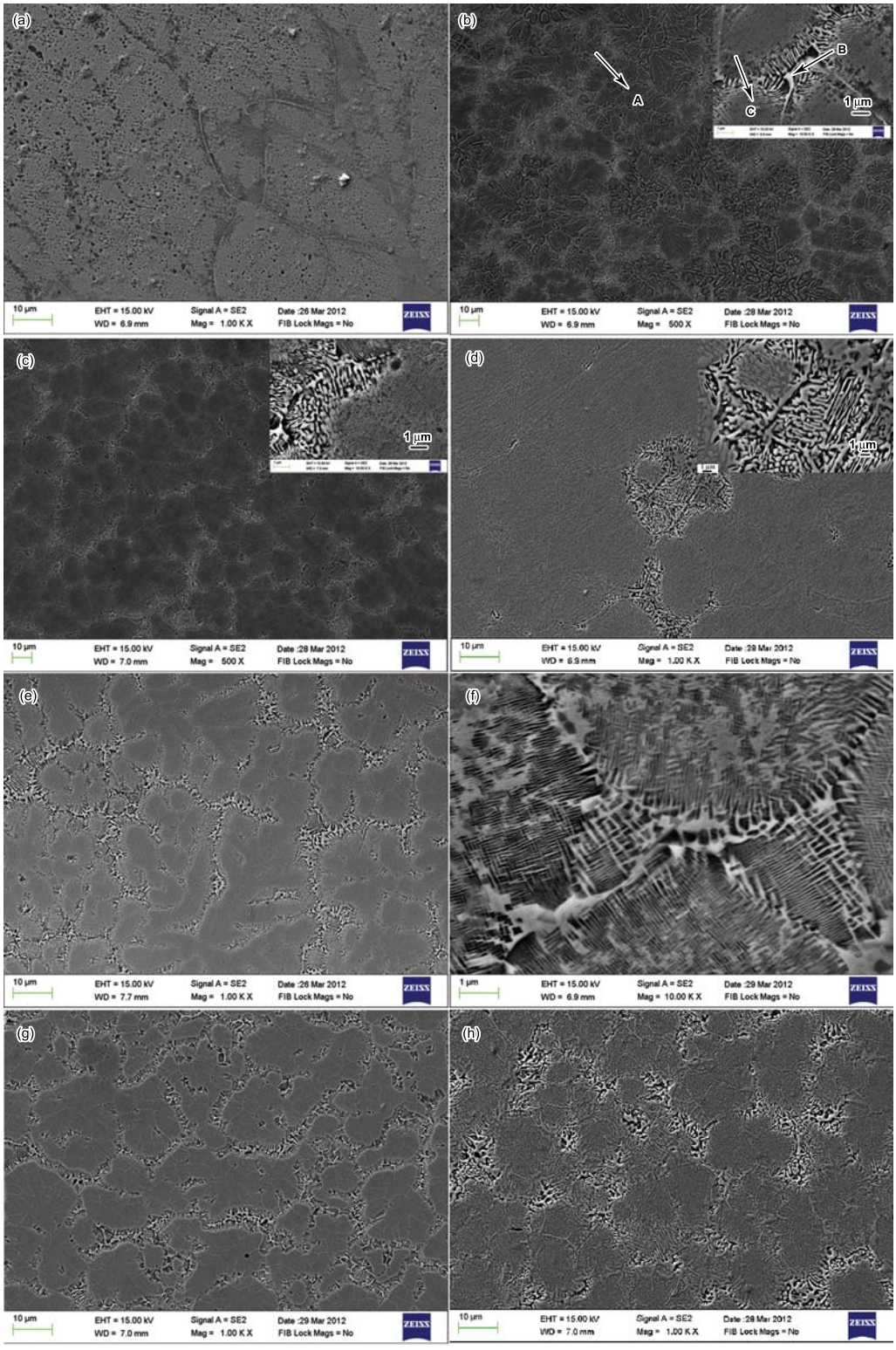

Fig. 2 SEM images of as-cast and annealed AlCoCrFeNiTi$_x$ alloys with different Ti additions: (a) as-cast Ti0.2; (b) Ti0.2 annealed at 500 °C; (c) Ti0.2 annealed at 700 °C; (d) Ti0.2 annealed at 900 °C; (e) as-cast Ti0.4; (f) Ti0.4 annealed at 500 °C; (g) Ti0.4 annealed at 700 °C; (h) Ti0.4 annealed at 900 °C (the insets in Fig. 2(b), (c) and (d) are the magnified images of the local regions)

nium is the main factor for the formation of the secondary phase in current alloys, and the increase of the content of the secondary phase results in a significant increase of the hardness[17]. The above analysis shows that AlCoCrFeNiTi$_x$ alloys have very high thermal stability and high hardness after high-temperature heat treatment.

In HEAs, there are more principal components than common alloys, and the component atoms have the same possibility to occupy the lattice

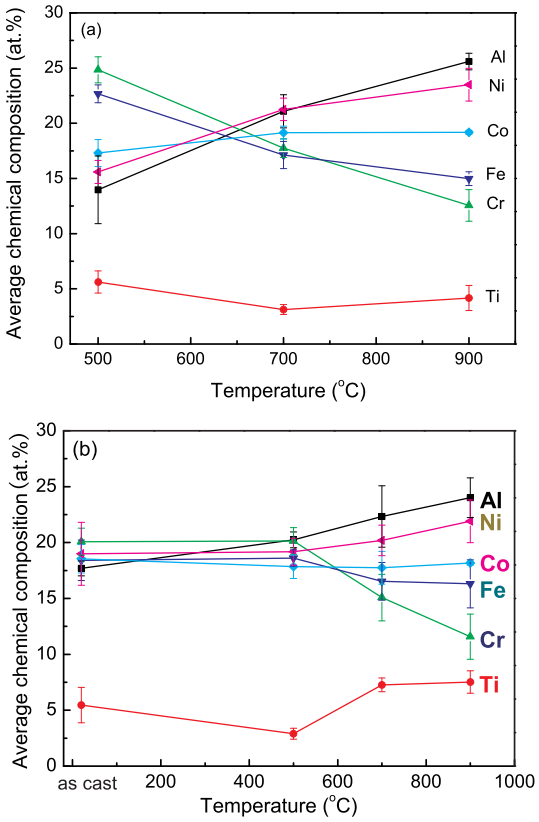

Fig. 3 Average composition of dendrite regions of Ti0.2 (a) and Ti0.4 alloys (b) as a function of annealing temperature

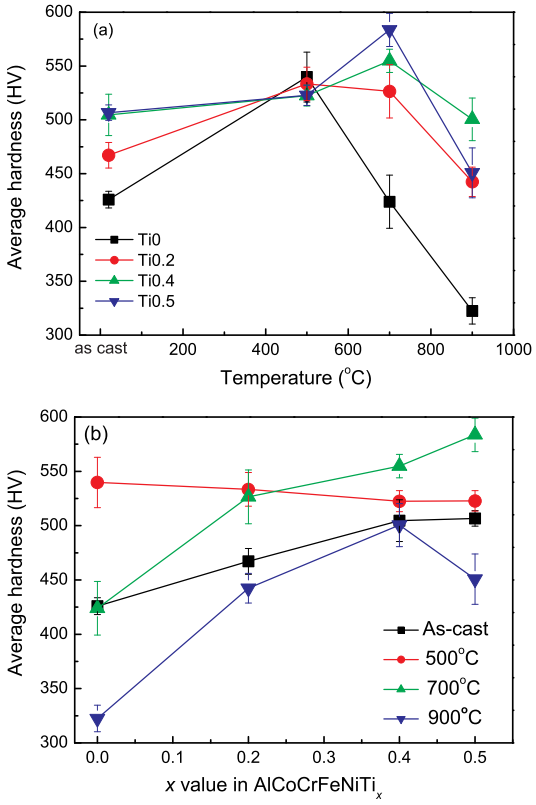

Fig. 4 Dependence of the average Vickers hardness of AlCoCrFeNiTi$_x$ (x=0, 0.2, 0.4, and 0.5) HEAs on the annealing temperature (a) and composition (b)

sites to form solid solution. Therefore, each component element could be considered as a solute atom, together with the serious lattice distortion caused by a large atomic radius difference between so many components, which make the structure of the solid solution in HEAs is different from that of pure metal and common alloys[1,18]. Here, the parameter Delta is used to describe the comprehensive effect of the atomic-size difference in multi-component alloys as follows[19]:

$$\delta = \sqrt{\sum_{i=1}^{N} c_i(1 - r_i/\bar{r})^2} \tag{3}$$

where r_i is the atomic radius, which can be obtained in Ref. [20], and $\bar{r}(= \sum_{i=1}^{n} c_i r_i)$ is the average atomic radius. By the calculation according to Eq. (3), the δ are of 0.0573, 0.0587, 0.0614 and 0.0648, respectively, when x = 0, 0.2, 0.4 and 0.5 for the AlCoCrFeNiTi$_x$ HEAs. The larger the δ value, the more serious the lattice distortion is. The atom radius of the element of Ti is the largest among Al, Co, Cr, Fe, Ni and Ti[20], which easily leads to the breakdown of the bcc structure of the AlCoCrFeNi HEA. As a consequence, the interdendritic phase precipitates along the grain boundary in AlCoCrFeNiTi$_x$ HEAs, which easily results in a large increase in hardness for the HEAs.

Fig. 4(b) shows the dependence of the average Vickers hardness of the as-cast and annealed AlCoCrFeNiTi$_x$ alloys on the composition. It is concluded that the alloys annealed at 500 °C and 700 °C show higher Vickers hardnesses than the as-cast ones and the alloys annealed at 900 °C. The Ti0.5 alloy annealed at 700 °C exhibits the highest Vickers hardness with a value of 583 HV. Generally, almost all the investigated alloys possess a highest hardness after 700 °C heat treatment, and the hardness of alloys decreases slightly when the alloys annealed at 900 °C. The excellent resistance to high temperature annealing softening is seldom gained in traditional alloys[21]. This effect is due to the precipitation of the hard phase in the annealed alloys.

A simple rule of mixtures is employed as an approximation for the hardness of HEAs with two bcc phases, simplified as follows:

$$HV = HV_{\mathrm{d}} f_{\mathrm{d}} + HV_{\mathrm{i}} f_{\mathrm{i}} \tag{4}$$

where HV, HV_{d} and HV_{i} are the hardnesses of HEAs, dendrites and interdendrites, respectively, and f_{d} and f_{i} are the volume fractions of dendrites and interdendrites, respectively.

From the SEM images of Ti0.2 and Ti0.4 alloys in Fig. 2, it can be observed that f_{i} increases and f_{d} decreases with the temperature. According to the

Table 1 Room-temperature compressive mechanical properties for as-cast and annealed Ti0, Ti0.2, Ti0.4 and Ti0.5 rod samples

Alloy	Microstructure	E(GPa)	σ_y(GPa)	σ_{max}(GPa)	ε_e(%)	ε_p(%)
Ti0(as cast)	bcc1 solid solution	136.1	1.39	4.43	0.8	24.4
Ti0(500°C)	bcc1 solid solution	125.8	2.07	3.67	1.3	14.4
Ti0(700°C)	bcc1 solid solution	188.3	1.57	3.25	0.6	15.9
Ti0(900°C)	bcc1 solid solution	65.8	1.07	3.52	1.2	30.4
Ti0.2(as cast)	bcc1 solid solution	110.5	1.71	3.57	1.3	20.7
Ti0.2(500°C)	bcc1+bcc2 solid solution	134.3	2.07	2.30	1.2	2.0
Ti0.2(700°C)	bcc1+bcc2 solid solution	73	1.54	1.85	1.7	1.9
Ti0.2(900°C)	bcc1+bcc2 solid solution	176.3	1.76	3.16	0.5	18.4
Ti0.4(as cast)	bcc1+bcc2 solid solution	119	1.97	3.72	1.1	21.0
Ti0.4(500°C)	bcc1+bcc2 solid solution	149.2	1.99	3.68	1.0	16.1
Ti0.4(700°C)	bcc1+bcc2 solid solution	81.6	1.69	2.02	1.7	1.2
Ti0.4(900°C)	bcc1+bcc2 solid solution	92.1	1.47	3.29	1.6	15.4
Ti0.5(as cast)	bcc1+bcc2 solid solution	122.3	1.93	4.68	1.4	29.6
Ti0.5(500°C)	bcc1+bcc2 solid solution	118.4	1.85	1.90	1.2	2.3
Ti0.5(700°C)	bcc1+bcc2 solid solution	127.1	1.80	1.67	1.0	0.5
Ti0.5(900°C)	bcc1+bcc2 solid solution	120.5	1.78	2.82	1.1	16.67

Note: E is Young's modulus; σ_y is yield stress; σ_{max} is fracture strength; ε_e is elastic strain; ε_p is plastic strain

composition changing in dendrite regions, as shown in Fig. 3, the elements Cr and Fe diffuse from dendrites to interdendrites, and the elements Al and Ni accumulate in dendrites with the increase of the temperatures. As known to all, the hardnesses of six elements have a sort order: Co>Ti>Cr>Ni>Fe>Al. Upon heat treatment, therefore, HV_i increases, and HV_d decreases. It is reasonable to understand why the hardness of HEAs increases with the temperature from room temperature to 700 °C. After 900 °C heat treatment, the hardness decreases, which may be due to the coarsened microstructures in interdendrites undergoing melting and re-solidification during this process[22].

3.4 Mechanical properties

Fig. 5 shows the room-temperature compressive engineering stress-strain curves of the alloy system. All the alloys exhibit fairly-high yield strength, fracture strength, plastic deformation and work hardening capacity, and the detailed mechanical properties for the alloy system are listed in Table 1. It is noted that the HEAs exhibit superior mechanical performances, compared with traditional crystalline alloys[10]. In Table 1, it can be observed that some HEAs have very low modulus, *e.g.*, 65.8 for Ti0 (900°C), 73 for Ti0.2 (700°C), 81.6 for Ti0.4 (700°C), while others can be 188.3. Fig. 5(a) shows the engineering stress-strain curves of the as-cast $AlCoCrFeNiTi_x$ (x = 0, 0.2, 0.4 and 0.5) HEAs. It can be seen that Ti0 alloy exhibits low yield strength and large plastic deformation. The further addition of Ti makes alloys gaining dramatically-enhanced strengths, but deteriorated plasticities. When Ti content increases to x = 0.5, the alloy exhibits excellent mechanical properties with high yield strength, fracture strength and plastic strain of 1.93 GPa, 4.68 GPa and 29.6%, respectively. Usually, the relationship between the yield strength

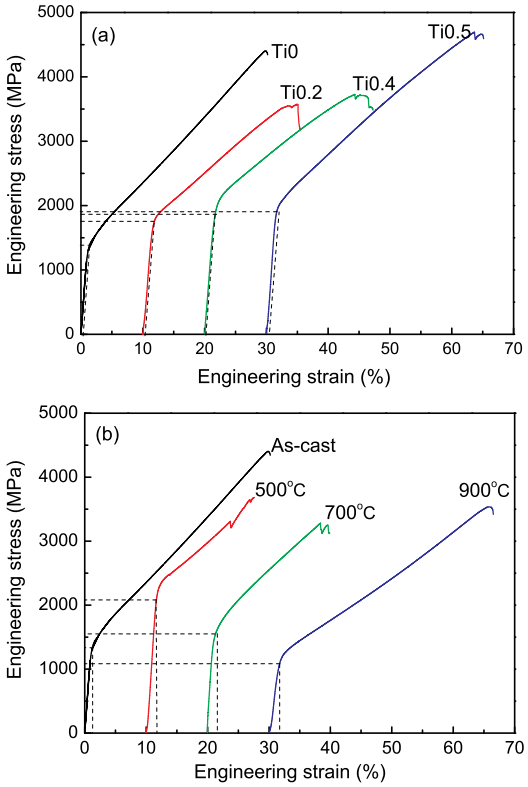

Fig. 5 Compressive engineering stress-strain curves of $AlCoCrFeNiTi_x$ alloys at room temperature: (a) as-cast Ti0, Ti0.2, Ti0.4 and Ti0.5 alloys; (b) as-cast and annealed Ti0 alloys

and the Vickers hardness is as follows[23]:

$$\sigma_y \approx 3HV \tag{5}$$

It is apparent that the varying tendency of yield strengths of the current alloys are corresponding with that of hardness.

The excellent mechanical properties of as-cast and

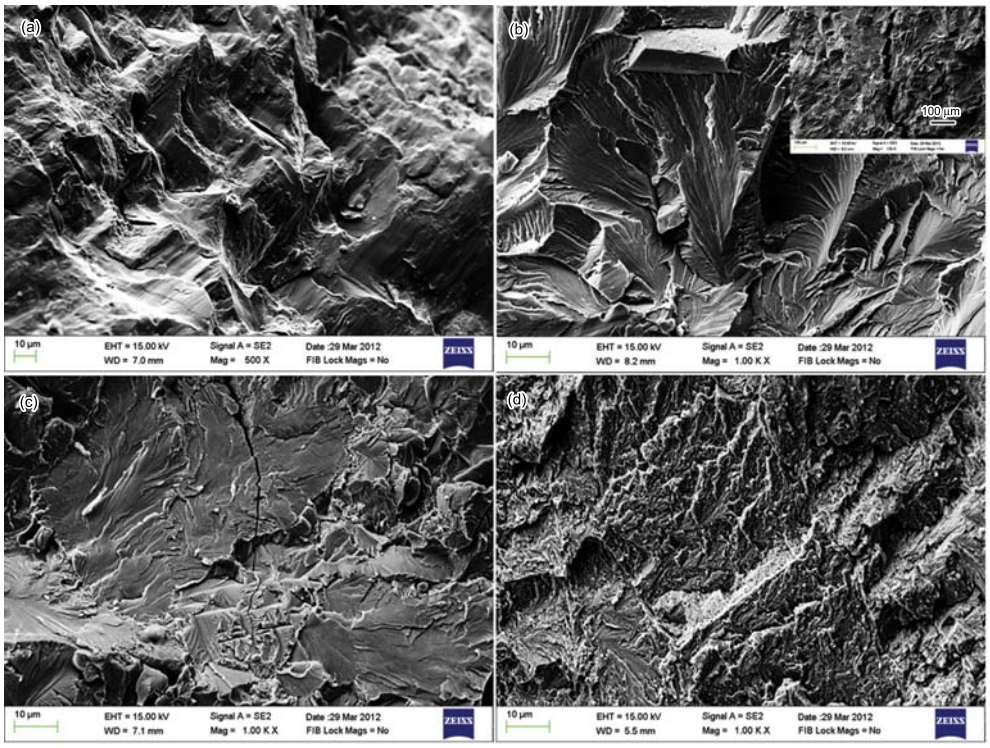

Fig. 6 Fracture morphologies of the Ti0 HEAs after different-temperature heat treatments: (a) and (b) as-cast; (c) 500 °C; (d) 900 °C

annealed alloys are attributed to the solid solution strengthening mechanism. For Ti0 alloy, the five components Al, Co, Cr, Fe and Ni are equi-atomic ratio and have the same probability to occupy the lattice sites to form bcc solid solution. As the element of Ti with a larger atomic radius occupies the lattice sites, the lattice distortion energy will increase significantly, and the effect of solid solution strengthening is enhanced. As a result, the strength greatly increases[10].

Fig. 5(b) exhibits the engineering stress-strain curves of the as-cast and annealed Ti0 HEAs. In contrast to the mechanical properties at different temperatures in Table 1, obviously, the Ti0 alloy annealed at 500 °C exhibits the optimal yield strength under room temperature with a value of as high as 2.07 GPa, much higher than that of the as-cast Ti0 alloy (1.39 GPa), together with extremely-high compressive strengths with a value of 3.67 GPa. However, the Ti0 alloy after 500 °C heat treatment shows deteriorated plasticity with a plastic strain of 14.4%, much lower than the as-cast Ti0 alloy (24.4%). The yield strength of the annealed alloy decreases with the heat treatment temperature, and it decreases abruptly to 1.07 GPa as the Ti0 alloy annealed at 900 °C. However the Ti0 alloy subjected to 900 °C heat treatment possess the highest compressive plasticity for the current $AlCoCrFeNiTi_x$ alloys, which is about 30.4%. It is concluded that these properties are even superior to the other annealed alloys and high-strength bulk alloys, *e.g.*, bulk metallic glasses and metallic glass matrix composites[24,25]. The high yield strength of the Ti0 alloy annealed at 500 °C may stem from the solid-solution strengthening effect and new secondary phase strengthening effect[26]. On the other hand, the nanoscaled modulated structure can enhance the strength of the annealed alloy. The excellent plasticity for the Ti0 alloy subjected to 900 °C heat treatment can be explained by high-temperature annealing softening[27], which leads to the increase of the plasticity and the strength of HEAs.

In order to better understand the mechanical behaviors of the as-cast and annealed HEAs, the detailed analysis of fractographs is necessary. Fig. 6 reveals the typical morphologies of the fractographs of the deformed as-cast Ti0 HEA and Ti0 HEAs after 500 and 900 °C heat treatments, respectively. The fracture morphologies of the as-cast Ti0 HEA are displayed in Fig. 6(a) and Fig. 6(b), respectively. It is clearly seen that the gliding steps on the fracture surface, indicative of plasticity[28], which is according with the room-temperature compressive plasticity of as-cast Ti0 mentioned before. Besides, from Fig. 6(b), many cleavage steps prevail on the fracture surface of as-cast Ti0 HEA. The crack, indicated by the white arrow in the inset of Fig. 6(b), is through the grain boundary, which is due to the release of the strain energy generated during the deformation process. It can be seen that the fracture mechanism of as-cast Ti0 high entropy alloy is concluded to be a transcrystalline fracture in cleavage fracture type at room temperature.

Fig. 6(c) is the fracture morphology of Ti0 alloy after 500 °C heat treatment. It is observed that many cleavage steps and crack dominate on the fracture sur-

face. There is no glide steps found, which suggests low plasticity. The result is in agreement with the low plasticity of Ti0 annealed at 500 °C in Fig. 5(b), and it can be obtained that the fracture mechanism of the alloy is similar to that of the as-cast Ti0 HEA.

Fig. 6(d) shows the fracture morphology of Ti0 alloy annealed after 900 °C heat treatment, and it is found that many cleavage planes and cleavage steps are available on the fracture surface. There may be exist strong nest-shape pits in the partial regions, which result in the increase of the plasticity. The fracture pattern of the alloy is a typical cleavage fracture.

4. Conclusions

In this study, $AlCoCrFeNiTi_x$ (x=0, 0.2, 0.4, 0.5) HEAs were prepared and subsequently annealed at 500, 700 and 900 °C for 2 h, respectively. Effects of Ti additions and heat treatment on the mechanical properties were studied. Only a bcc solid solution appears in the as-cast Ti0.2 alloy, and there is a new secondary phase precipitated from the solid solution matrix in the $AlCoCrFeNiTi_x$ HEAs with increasing Ti content and heat treatment temperature. Obvious elemental segregation can be detected in the dendrite and interdendrite regions for both annealed Ti0.2 alloys and as-cast and annealed Ti0.4 alloys. Cr, Fe and Ti spread outside the dendrites with increasing temperature, leading to the dendrite region enriched with Al and Ni while the interdendrite region enriched with Cr and Fe.

The $AlCoCrFeNiTi_x$ HEAs possess excellent room-temperature mechanical properties, and the mechanical properties of this alloy system have a strong correlation with the Ti additions and heat treatment temperature. All the alloys with Ti additions have higher hardness than Ti0 alloys except for the alloys after 500 °C heat treatment. The alloys after 500 and 700 °C heat treatment have high Vickers hardnesses and yield strengthes, and the as-cast alloys and the alloys after 900 °C heat treatment exhibit great plasticities. For the Ti0.5 alloy annealed at 700 °C exhibits the highest Vickers hardness with a value of 583 HV, and the Ti0 alloy annealed at 500 °C exhibits the highest yield strength while the Ti0 alloy annealed at 900 °C shows the best plasticity, about 2.07 GPa and 30.4%, respectively. The solid solution strengthening mechanism of Ti additions is considered to be a key factor for the strengthening effect of HEAs. As the Ti with a larger atomic radius occupies the lattice sites, the lattice distortion energy will increase significantly and the effect of solid solution strengthening is enhanced, thus the strength greatly increases.

Acknowledgements

This work was financially supported by the National Natural Science Foundation of China (No. 51101110), the Youth Science Foundation of Shanxi Province, China (No. 2012021018-1), Research Project Supported by Shanxi Scholarship Council of China (No. 2012-032) and State Key Lab of Advanced Metals and Materials (Grant No. 2011-Z06).

REFERENCES

[1] J.W. Yeh, S.K. Chen, S.J. Lin, J.Y. Gan, T.S. Chin, T.T. Shun, C.H. Tsau and S.Y. Chang, Adv. Eng. Mater. **6** (2004) 299.
[2] J.M. Zhu, H.F. Zhang, H.M. Fu, A.M. Wang, H. Li and Z.Q. Hu, J. Alloys Compd. **497** (2010) 52.
[3] K.B. Zhang, Z.Y. Fu, J.Y. Zhang, W.M. Wang, H. Wang, Y.C. Wang, Q.J. Zhang and J. Shi, Mater. Sci. Eng. A **508** (2009) 214.
[4] Y. Zhang, S.G. Ma and J.W. Qiao, Metall. Mater. Trans. A **43** (2012) 2625.
[5] Y.J. Zhou, Y. Zhang, Y.L. Wang and G.L. Chen, Mater. Sci. Eng. A **454–455** (2007) 260.
[6] Y.P. Wang, B.S. Li, M.X. Ren, C. Yang and H.Z. Fu, Mater. Sci. Eng. A **491** (2008) 154.
[7] T.T. Shun and Y.C. Du, J. Alloys Compd. **479** (2009) 157.
[8] J.M. Zhu, H.M. Fu, H.F. Zhang, A.M. Wang, H. Li and Z.Q. Hu, Mater. Sci. Eng. A **527** (2010) 7210.
[9] J.W. Qiao, S.G. Ma, E.W. Huang, C.P. Chuang, P.K. Liaw and Y. Zhang, Mater. Sci. Forum. **688** (2011) 419.
[10] Y.J. Zhou, Y. Zhang, Y.L. Wang and G.L. Chen, Appl. Phys. Lett. **90** (2007) 181904.
[11] C.M. Lin, H.L. Tsai and H.Y. Bor, Intermetallics **18** (2010) 1244.
[12] S. Ranganathan, Curr. Sci. **8** (2003) 1404.
[13] C.J. Tong, Y.L. Chen, S.K. Chen, J.W. Yeh, T.T. Shun, C.H. Tsau, S.J. Lin and S.Y. Chang, Metall. Mater. Trans. A **36** (2005) 881.
[14] A. Takeuchi and A. Inoue, Mater. Trans. **46** (2005) 2817.
[15] F.R. Doer, R. Boom, W.C.M. Mattens, A.R. Miedema and A.K. Niessen, Cohesion in Metals, 2nd ed., North-Holland Physics Publishing, Netherlands, 1988.
[16] C.M. Lin and H.L. Tsai, Intermetallics **19** (2011) 288.
[17] W.R. Wang, W.L. Wang, S.C. Wang, Y.C. Tsai, C.H. Lai and J.W. Yeh, Intermetallics **26** (2012) 44.
[18] Y. Zhang, Y.J. Zhou, J.P. Lin, G.L. Chen and P.K. Liaw, Adv. Eng. Mater. **10** (2008) 534.
[19] S.S. Fang, X.S. Xiao, L. Xia, W.H. Li and Y.D. Dong, J. Non-Cryst. Solids **321** (2003) 120.
[20] C. Kittel, Int. to Solid State Phys. 6th ed, John Wiley & Songs. Inc, New York, 1980, p.26.
[21] O.E. Sebaie, A.M. Samuel, F.H. Samuel and H.W. Doty, Mater. Sci. Eng. A **486** (2008) 241.
[22] C. Ng, S. Guo, J.H. Luan, S.Q. Shi and C.T. Liu, Intermetallics, 31(2012) 165.
[23] J. Rösler, H. Harders and M. Bäker, Mechanical Behaviour of Engineering Materials, Springer Berlin Heidelberg, New York, 2007.
[24] A. Inoue, Mater. Sci. Eng. A **304–306** (2001) 1.
[25] J.W. Qiao, S. Wang, Y. Zhang, P.K. Liaw and G.L. Chen, Appl. Phys. Lett. **94** (2009) 151905.
[26] Y. Zhang, X. Yang and P.K. Liaw, JOM **64** (2012) 830.
[27] C.Y. Hsu, C.C. Juan, W.R. Wang, T.S. Sheu, J.W. Yeh and S.K. Chen, Mater. Sci. Eng. A **528** (2011) 3581.
[28] J.W. Qiao, Y. Zhang and P.K. Liaw, Adv. Eng. Mater. **10** (2008) 1039.